



Article

Mineralogical Study of Levels with Magnesian Clay Minerals in the Santos Basin, Aptian Pre-Salt Brazil

Maurício Dias da Silva ¹, Márcia Elisa Boscato Gomes ¹, André Sampaio Mexias ^{1,*}, Manuel Pozo ², Susan Martins Drago ¹, Raquel Severo Célia ¹, Luis Adriano Carvalho Silva ¹, Paulo Netto ^{3,4}, Lucas Bonan Gomes ¹, Carla Cristine Porcher ¹, Norberto Dani ¹, Deborah Driemeyer ¹, Camila Wense Dias Ramnani ⁵ and Julice Ferreira Santos ⁵

¹ Geoscience Institute, Federal University of Rio Grande do Sul, Av. Bento Gonçalves 9500, 91501-970 Porto Alegre, Brazil; mauriciodias95@hotmail.com (M.D.d.S.); marcia.boscato@ufrgs.br (M.E.B.G.); susan.drago@gmail.com (S.M.D.); Raquel.sev.celia@gmail.com (R.S.C.); luiscarvalho.ds@gmail.com (L.A.C.S.); lucas.gomes@ufrgs.br (L.B.G.); carla.porcher@ufrgs.br (C.C.P.); norberto.dani@ufrgs.br (N.D.); deborahdriemeyer@gmail.com (D.D.)

² Department of Geology and Geochemistry, Universidad Autónoma de Madrid, Av. Francisco Tomás y Valiente, 7, 28049 Madrid, Spain; manuel.pozo@uam.es

³ Petrobras S. A., Av Henrique Valadares 28, 20231-030 Rio de Janeiro, Brazil; pnetto@petrobras.com.br

⁴ Geoscience Institute, Federal University of Rio de Janeiro, Av. Athos da Silveira Ramos 274, 21941-916 Rio de Janeiro, Brazil

⁵ Petrobras Research and Development Center (Cenpes), Av. Horácio Macedo 950, 21941-915 Rio de Janeiro, Brazil; camila.wense@petrobras.com.br (C.W.D.R.); julifersan@petrobras.com.br (J.F.S.)

* Correspondence: amexias59@gmail.com



Citation: da Silva, M.D.; Gomes, M.E.B.; Mexias, A.S.; Pozo, M.; Drago, S.M.; Célia, R.S.; Silva, L.A.C.; Netto, P.; Gomes, L.B.; Porcher, C.C.; et al. Mineralogical Study of Levels with Magnesian Clay Minerals in the Santos Basin, Aptian Pre-Salt Brazil. *Minerals* **2021**, *11*, 970. <https://doi.org/10.3390/min11090970>

Academic Editor: Warren D. Huff

Received: 2 August 2021

Accepted: 1 September 2021

Published: 6 September 2021

Publisher's Note: MDPI stays neutral with regard to jurisdictional claims in published maps and institutional affiliations.

Abstract: The object of this study is magnesian clay minerals present in carbonate rocks of the post-rift phase of the pre-salt in the Santos Basin. These rocks developed in an Aptian-age alkaline lacustrine environment. This study summarizes the formation of clay minerals associated with different lithotypes in a range of 19 m and a depth of more than 5100 m. They were characterized from petrographic analysis by optical microscopy, X-ray diffraction (total sample and clay fraction), and modeling by Newmod[®]; and examined and analyzed by scanning electron microscopy. An approach based on identifying lithotypes and characterization of microsites allowed us to understand the occurrence of different clay minerals. Kerolite was the most abundant mineral in the sampled range. It occurs in lamellar aggregates under greater preservation of the original rock lamination and in association with spherulites and shrubs. The Stv/Ker mixed layers occurs in the same association, and formed finer unlaminated aggregates associated with the more intense dolomitization and silicification processes. Saponite occurs associated with detrital minerals forming clayey levels intercalated with microcrystalline carbonates. Fluids with a high Mg/Si and pH < 9 favor the precipitation of kerolite. The increase in pH during diagenesis may be responsible for the formation of Stv/Ker mixed layers.

Keywords: Santos Basin; pre-salt; Mg clays; kerolite; stevensite/kerolite mixed layer; saponite



Copyright: © 2021 by the authors. Licensee MDPI, Basel, Switzerland. This article is an open access article distributed under the terms and conditions of the Creative Commons Attribution (CC BY) license (<https://creativecommons.org/licenses/by/4.0/>).

1. Introduction

Magnesian clay minerals are a diverse group that can occur in sedimentary and non-sedimentary contexts [1]. The knowledge about magnesian clay minerals from the lacustrine environment comes mainly from studies of large deposits such as Amargosa (USA) [2], Jbel Rhassoul (Morocco) [3], and the Madrid Basin (Spain) [4], where they are markers of specific physicochemical conditions.

The magnesian clays belong to two families: the 2:1 minerals (kerolite, stevensite, and saponite); and the fibrous minerals (sepiolite and palygorskite). Saponite and palygorskite contain more aluminum than stevensite, kerolite, and sepiolite. For this reason, they are

generally considered as resulting from the reaction between detrital minerals and Si- and Mg-rich solutions [5], while stevensite, kerolite, and sepiolite are formed by direct precipitation from solutions.

This study addresses clay minerals that constitute the matrix of the carbonate rocks of post-rift phase deposits of the Santos Basin in the Brazilian pre-salt. The Barra Velha Fm of the Santos Basin is one of the most important hydrocarbon reservoirs in this context.

The clay minerals in the pre-salt rocks are understood as syngeneic precipitates, commonly described and interpreted generically as magnesian minerals, and the term “stevensitic clays” is recurrent in macro- and microscopic descriptions of the matrix of these carbonate rocks. Some authors define these minerals as stevensites [6–9], while others propose the occurrence of a broader range of clay minerals that includes kerolite, stevensite, saponite, sepiolite, illite, kerolite/smectite, and illite/smectite [10–12]. Most authors conducted these studies on reservoir rocks that had a lower degree of clay mineral preservation.

Determining what magnesian clay minerals are present, as well as the processes and conditions of their preservation and/or transformation, were the main goals of this research.

Fundamental to this study was the sampling of a non-reservoir interval and the petrographic approach at the microsite level in the different lithotypes proposed. Mineralogical, chemical, morphological, and structural data were collected using XRD, SEM, and EDS microanalyses.

Using this approach, we identified distinct mineral assemblages preserved and/or transformed by diagenetic processes.

2. Geological Setting

At the end of Jurassic and the beginning of Cretaceous, there was a reactivation of geological faults in the region of the rift belt conditioned to a new regime that would culminate in the opening of the Gondwana paleocontinent. This extensional regime was responsible for the creation and tectonic evolution of the Brazilian marginal basins and the extensive tholeiitic magmatism of the Paraná Basin [13,14].

The Santos Basin in general has its tectonostratigraphic evolution subdivided into three supersequences: rift, post-rift, and drift [15]. The post-rift or sag phase, understood as a transitional continental–marine episode, dates from the Aptian stage and comprises the alkaline lacustrine deposits of the Barra Velha Formation and the evaporites of the Ariri Formation. As in Santos, the Campos Basin shares a similar evolutionary sequence (Figure 1), delimited by the Pre-Alagoas Unconformity at the end of the rift stage [15–17].

The rocks of the Barra Velha Formation and its equivalent in Campos, Macabú, consist of laminated carbonates with intercalation of clay material, which occur in situ or reworked. The main components of these rocks are spherulites, shrubs, intermediate forms, and a matrix composed of magnesian clay minerals and variable amounts of inherited siliciclastic grains. Some detailed studies of the composition, diagenesis, and other processes reported a regular variation defined as an ideal/basic cycle of facies intercalation for these rocks. This cycle is composed of the succession of mudstone, calcite spherulite levels, and shrub levels [7,8,12,18–22].

The pre-salt clay minerals are lamellar minerals that constitute the matrix, as argillaceous peloids included in other constituents or as ooids and/or intraclasts of sandstones from reworked portions. These clay minerals are understood as syngenetic precipitates that make up the matrix of these carbonate rocks, which are sometimes also composed of detrital minerals. Some works attribute the nomenclature of stevensite to the matrix of pre-salt rocks [6,8,9,23], while others propose a broad scope of these occurrences in the Barra Velha Formation of the Santos Basin, which includes kerolite, stevensite, saponite, sepiolite, illite, kerolite/smectite, and illite/smectite [10,11,24]. Another study in the Campos Basin reported illite/smectite and smectite/chlorite [25].

Chronostratigraphy (GTS-2012)				Lithostratigraphy		Unconformities		
				Santos	Campos			
MESOZOIC	CRETACEOUS	LOWER CRETACEOUS	Aptian	Alagoas	Ariri	Retiro		
			115					
			118		Barra Velha	Macabu	Intra-Alagoas	
			126	Jiquiá	Itapema	Coqueiros	Pre-Alagoas	
			Barremian	Buracica	Piçarras	Atafona	Top Lower Rift	
			131	Aratu	Camboriú	Cabiúnas	Top Camboriú	
		Hauterivian						

Figure 1. Eo-Cretaceous stratigraphy of the Santos and Campos basins. From Wright and Barnett [21], modified from Moreira et al. [15].

Magnesian clay minerals are known to be quite susceptible to modification by processes such as diagenesis and hydrothermal alteration [7,8]. Tosca and Wright [26] studied and defined mineral assemblages that contain calcite and dolomite associated with Mg clays. In their understanding, stevensite precipitates directly from a Si^{4+} and Mg^{2+} rich gel, and therefore would be the earliest mineral present in these rocks. Throughout the precipitation and accumulation of clay minerals, it is suggested that interstratification occurs between stevensite and kerolite. Subsequently, physicochemical fluctuations caused by the onset of diagenesis promote greater organization of the kerolite member of the interstratified that would pass to talc.

Despite the considerable number of studies, the clay minerals that constitute these rocks have been little studied from a composition and structure point of view. Furthermore, investigations of the clayey or non-reservoir levels have not yet been considerably explored.

3. Materials and Methods

This work was focused on and carried out in a drill core, named S2 and measuring 19 m, from which 21 samples were selected from the non-reservoir portion that presented better preservation of clay minerals in different assemblages. Twenty-five petrographic thin sections and six thick petrographic sections (100 μm) were prepared at the Sample Preparation Laboratory IGEO-CPGq-UFRGS (Institute of Geosciences, Center of Petrology and Geochemistry Studies, Federal University of Rio Grande do Sul) and PetrografiaBR-MG. Petrographic analyses were performed on a polarized transmitted light microscope (MEIJI ML9000L Polarizing Microscope, Japan) at the Department of Mineralogy and Petrology at IGEO-UFRGS.

For X-ray diffractometry, we used a Siemens diffractometer (BRUKER AXS, Karlsruhe, Germany), model D-5000 (θ - θ) equipped with graphite monochromator in the secondary beam and fixed anode tube, operating at 40 kV and 30 mA ($\text{CuK}\alpha$ radiation = 1.5406 Å) of the LXRd (Laboratory of X-Ray Diffractometry, IGEO-CPGq-UFRGS). Divergence and anti-scattering slits of 1 and 0.2 mm were used in the detector. For the study, samples were prepared in total rock powder and clay fraction (<2 μm). The analyses in total rock were performed with the finely ground and disoriented powder.

For the clay mineral analyses, the clay fraction was separated by sedimentation (Stokes' law, suspension in deionized water) associated with centrifugation. The samples were initially agitated in an orbital system for 12 h and then by ultrasonic vibration for 10 min. Then, natural-oriented slides (air-dried-AD) were prepared, saturated in ethylene glycol (EG), and heated at 490 and 550 °C (H). The after-heating ethylene glycol saturation approach was applied [27]. Parameter "b" was also analyzed in each sample through reflection (060) after a careful process of disorientation of the particles using a 63 µm sieve with a delicate brush, causing the particles to fall into the sample holder in a disoriented way ("house of cards").

The angular intervals and steps for each type of analysis were: total rock, 2.3–72°2θ in 0.02° steps, and 1 s of time for each step; clay fraction, (<2 µm) 2.3–28°2θ in steps of 0.02°/5 s (air-dried and heated), and 6 s for the sample saturated with ethylene glycol; and parameter "b" analysis (060), 58–64 °2θ in steps of 0.02°/20 s.

A mathematical deconvolution process of the (001) (4 to 12°2θ) and (060) (58 to 64°2θ) reflections was applied. The first step was the preliminary identification of the minerals in the sample. The second step was smoothing of the X-ray pattern (K = 3, 7-point average). The third step was the subtraction of background noise from the smoothed pattern, thus eliminating the effect of the Lorentz polarization factor. The fourth step consisted of calculating the curves following the Gaussian and Lorentzian mathematical models that best fit the experimental pattern, evaluated through the lowest residue obtained. The calculations followed the least-squares or simplex nonlinear down-hill method. The fifth step was the interpretation of the results obtained, mainly based on the mineralogy estimated in the initial step of the process. The maximum number of elemental curves used in the deconvolution process for most samples studied was three for the (001) reflection and five for the (060) reflection.

Some diffractograms were calculated using the Newmod[®] program [28] to test and compare some theoretical interstratified arrangements with those obtained. The most appropriate numbers of diffraction layers (N) for the (001) reflection of smectites (stevenites/saponites) and kerolites were also compared.

Secondary electron (SE), backscattered electron (BSE), and chemical analyses by energy dispersive spectroscopy (EDS) were performed in the scanning electron microscope (SEM) of the Isotopic Geology Laboratory of UFRGS (LGI) of the Center of Petrology and Geochemistry Studies of the Geosciences Institute (CPGq-IGEO), model Jeol JSM-6610-LV (Tokyo, Japan), equipped with a Bruker XFLASH 5030 EDS detector.

For the study, eight polished slides were C-metalized for chemical and textural study at a voltage of 15 eV and 10 nA, and seven fragment samples prepared with double Au-C metallization aiming morphological images at a voltage between 8 and 15 keV and 10 nA, with an analytical error around 3–5%.

4. Results

4.1. Petrography

The classification by Gomes et al. [22] presented an adequate approach for the diversity of lithologies present in the pre-salt. However, the present study adopted a methodology that evaluated the clay minerals in different assemblages and had no direct correspondence with this classification, requiring a petrographic quantification of constituents and/or porosity. In addition, the sampling was performed by focusing on more clayey levels, and therefore the term used here is lithotype rather than facies, since the approach here referred to the main carbonate constituent of the level, and did not have a direct correspondence with the sedimentological and/or stratigraphic processes for this rock sequence. Thus, lithotypes served primarily as an indication of the composition and organization of the levels in which the clays were studied.

4.1.1. Main Components

Mud: The sampled intervals correspond to rocks with high clay content. For this reason, all samples present a matrix rich in clay minerals in different preservation conditions. The rock matrix is composed of clay minerals arranged in parallel aggregates forming the main lamination of the rock. These could be the sole constituent or be associated with detrital minerals, forming a hybrid matrix.

When the matrix is composed only of clay minerals, these are mostly yellowish-brown, with lamellar habit and high (3rd order) birefringence, forming aggregates with a continuous optical orientation of the particles parallel to the rock lamination. Less abundantly, clay minerals occur as non-laminated aggregates of very fine particles in massive or chaotic arrangements, with low (1st order) birefringence. Associated with these, locally nodular aggregates with very low birefringence appear. Included in the spherulites and shrubs, peloids of similar composition to the clay matrix commonly occur. Bioclastic constituents occur in small proportions in most rocks. The most important are phosphatic bioclasts, spherical clay-walled organisms, and ostracods.

Levels with a hybrid matrix occur preferentially in the laminite lithotype, and also occur at the spherulite lithotype level. This matrix consists of yellow-greenish clay minerals with low birefringence (1st order) and detrital minerals such as quartz, feldspar, mica, and green clay aggregates.

Spherulites: These are the most abundant constituents of the rocks, and occur as precipitates displacing the lamination of the clay matrix. They are calcitic, and have an approximately spherical shape composed of a fibro-radiated internal structure and a diameter ranging from 0.4 to 1 mm, rarely greater than 1 mm. They often occur in association with calcitic microcrystalline carbonates smaller than 0.4 mm in the form of lenticular aggregates and without fibro-radiated structuring. Spherulites and microcrystalline carbonates are interpreted as eo-diagenetic products by the features of displacement and replacement of the matrix by these constituents, in addition to the low degree of compaction seen in these intervals.

Shrubs: These are important constituents that occur independently of the spherulites. They are calcitic, have a fascicular crustal shape with growth toward the top of the lamination, and have sizes on average greater than 2 mm. The shrub-rich levels show a non-laminated structure; these constituents possibly precipitated simultaneously with the matrix, but at higher growth rates than the clay minerals, resulting in matrix preservation only in interstitial portions of these constituents. Transitional forms between spherulites and shrubs occur in spherulite levels and present irregular concentric morphologies. The internal structuring indicates growth towards the top of the succession.

In addition to these constituents, diagenetic minerals formed from the transformation of the clay minerals and/or carbonates. Silicification processes formed microcrystalline and macrocrystalline quartz, as well as microspherulitic chalcedony. Dolomitization produced rhombohedral, xenomorphic, and microcrystalline dolomite, and magnesite bands concordant to lamination. Microcrystalline and framboidal pyrite also present. The porosity is inexpressive, and when observed in thin sections, it seems to be an artifact of the slide preparation.

4.1.2. Lithotypes

The lithotypes were proposed in order to contextualize the paragenesis of clay minerals. Three lithotypes were proposed: spherulstone (E), shrubstone (S), and laminate (L), based on the respective predominance of spherulite, shrubs, and the intercalation of levels of microcrystalline calcite and clay minerals. In addition to this designation, an index was added to qualify the significant presence of dolomitization (d) and silicification (s). The levels classified as E are predominant in the sampled interval. These levels are essentially composed of calcite spherulites and clay minerals (Figure 2A). The largest quantities of clay minerals are found in this lithotype, especially related to the configuration, size, and quantity of the spherulites. The spherulites, in general, are well preserved, keeping their internal crystallographic orientation and suffering neomorphism in triangular sectors. Lo-

cally, stylolitic surfaces are developed, forming amalgamated and intensely recrystallized carbonate levels. In other cases, levels of dolomitization (Figure 2B) and/or partial silicification of these constituents occur. It is not uncommon for spherulites to present irregularly turbid internal portions, and, in some levels, all spherulites present this feature. Transitional forms between spherulites and shrubs also are associated with E levels, especially in the vicinity of S levels, but they are heterogeneously distributed, and in some cases, could be confused with amalgamated or more intensely recrystallized spherulites. Intraclasts of cryptocrystalline calcite occur locally. The clay minerals present in this lithotype occur as aggregates of the particles with optical continuity and high birefringence (3rd order). Chaotically oriented fibrous aggregates with low birefringence (1st order) occur locally. The presence of an E level in which a hybrid matrix occur is associated with L lithotype levels.

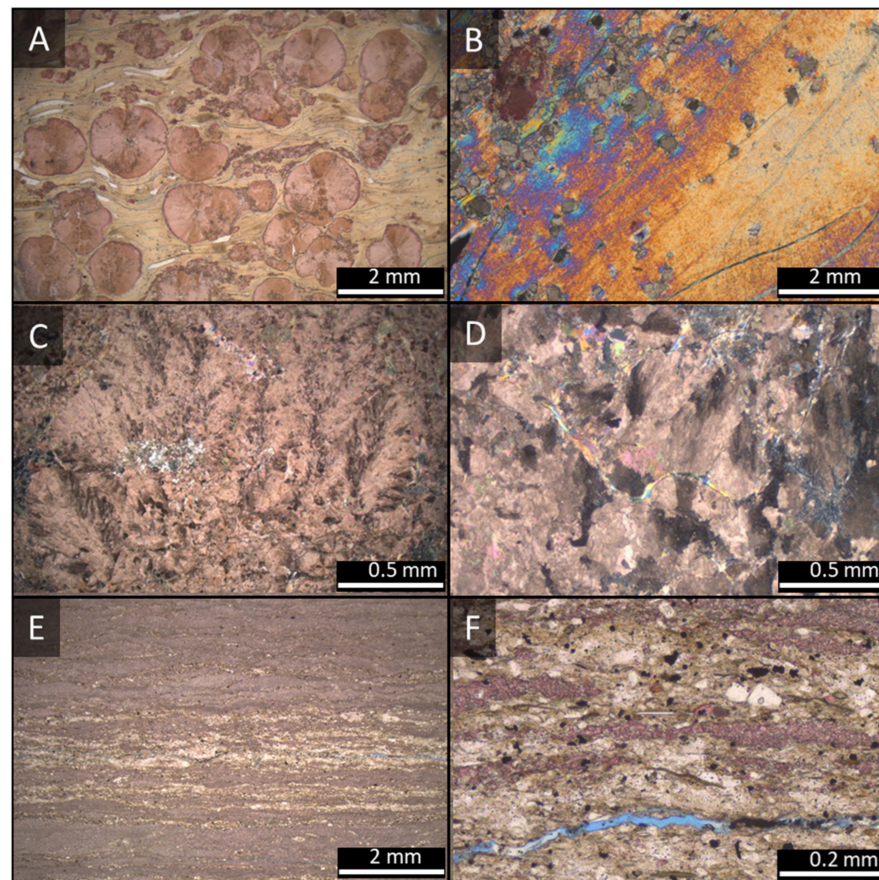


Figure 2. Photomicrographs of main aspects of the lithotypes. Lithotype E: (A) well-laminated yellowish-brown clay minerals and calcite spherulites; (B) detail of partial dolomitization in clay aggregate. Lithotype S: (C) general aspect of shrubs with little interstitial clay minerals; (D) thin lamellar, high-birefringence clay aggregates disturbed by the shrub growth and non-lamellar aggregates of finer, chaotic, low birefringence clays (arrow). Lithotype L: (E) hybrid matrix levels intercalated with microcrystalline calcite (pink ink); (F) detail of the hybrid matrix composed of magnesian clay minerals, quartz, feldspars, and micas, replaced by microcrystalline calcite (pink ink) and pyrite.

The predominance of calcite shrubs (fascicular crusts) defines the S levels (Figure 2C). These levels do not present laminations because these carbonates probably precipitated simultaneously or alternately with clay minerals. The matrix of this lithotype occurs in the interstices between one shrub and another. This interstitial matrix is composed of lamellar clay minerals of high birefringence (3rd order) associated with non-laminated aggregates that sometimes form nodular aggregates of very low birefringence, both with yellowish-brown coloration (Figure 2D).

A fine-grained parallel lamination characterizes the L lithotype. It is the result of the intercalation of hybrid levels of clay minerals and siliciclastic materials (quartz, mica, feldspar, and aggregates of green clays, possibly celadonite or nontronite), with levels of microcrystalline calcite (Figure 2E,F). These levels' magnesian syngenetic clay minerals are yellow-greenish, low (1st order) birefringence, and lamellar habit, and form aggregates without optical continuity parallel to the rock lamination. In these intervals, pyrite occurs heterogeneously disseminated. Rich levels of amorphous organic matter occur in the contacts between one lamination and another, resulting in a dark brown color of these levels.

In the E and S lithotypes, the matrix and spherulites are partially replaced, forming macrocrystalline mosaics and/or microcrystalline silica and microspherulitic chalcedony.

In exceptional cases, intense dolomitization levels (d) occur, forming carbonate lenses (dolomite and magnesite) (Figure 3A) and xenomorphic microcrystalline dolomites. Irregular portions of laminated cryptocrystalline dolomite pseudomorphically replace the clay matrix (Figure 3B). Intense silicification (s) occur, forming silica bands replacing clay minerals (Figure 3C,D), and sometimes coating pre-existing carbonates, including dolomite and magnesite. In this classification, only the levels with such intensity of the processes received the index (d) and/or (s). Even under these conditions of intense transformation, residual clay minerals of these processes are found.

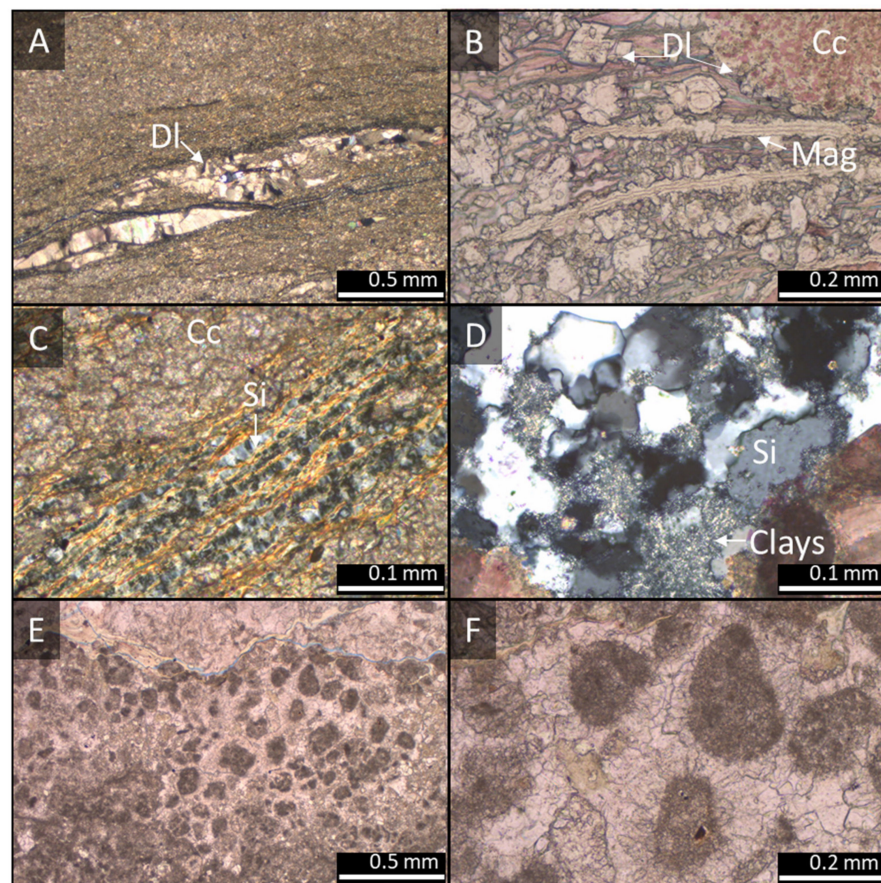


Figure 3. Photomicrographs of main aspects of the diagenetic products: (A) carbonate lenses in laminated rock replaced by microcrystalline dolomite; (B) detail of the intense replacement of the matrix and the spherulites by microcrystalline dolomite and magnesite bands; (C) partial replacement of the laminated matrix by microcrystalline quartz in parallel bands; (D) detail of the interstitial matrix transformation to chaotic fibrous aggregates and general replacement by quartz; (E) general aspect of lumpy aggregates and peloidal level of the 3215 sample; (F) detail of the cryptocrystalline peloids replaced and cemented by calcite. Cc = calcite; Si = silica; Dl = dolomite; Mag = magnesite.

In this sampling, there is the occurrence of a level defined as peloidal (P) (Figure 3E,F). This refers to intervals of cryptocrystalline and lumpy calcite intraclasts, of probable microbial origin. These lumpy aggregates, with partial reworking, form intraclasts with a maximum dimension of 3 mm replaced and cemented by macrocrystalline calcite.

4.2. Mineralogical Characterization

The following results are presented and discussed according to three populations established by lithotype composition and associated clay minerals: Population 1, defined by samples 1515, 1955, and 3085 of lithotypes E and S with a pure syngenetic matrix with intense dolomitization (d) and silicification (s) processes; Population 2, defined by samples 3215, 3690, and 3850 of lithotypes E and S with pure syngenetic matrix little impacted by transformation processes; and Population 3, defined by samples 3750 and 4415 with a hybrid matrix with a predominance of lithotype L.

4.2.1. Population 1

Population 1 is represented by three samples with a pure syngenetic matrix. These samples are characterized by intense dolomitization and/or silicification processes with distinct intensities that resulted in different degrees of clay mineral preservation.

Sample 1515 is composed only of the Es lithotype, with intense silicification capable of replacing clay levels forming bands of microcrystalline quartz with orientation parallel to the rock lamination (Figure 4A). Dolomitization partially replaces the clay matrix, forming rhombohedral crystals, and corrodes the spherulites, forming microcrystalline dolomite. Silicification overlaps the dolomitization process by coating part of the spherulites and dolomites present in the matrix (Figure 4B,C).

Sample 1955 shows an even higher degree of these processes, resulting in little preservation of the clay minerals (Figure 4D). The dolomitization culminated in the formation of magnesite, which commonly completely replaces the residual clay mineral laminations. The degree of dolomitization of this sample does not allow precise lithotype identification. However, the fine grain size and absence of shrubs and/or spherulites allowed it to be defined as Lds, referring to dolomite and silica recrystallization.

Sample 3085 differs from both in that it presents an Ss lithotype level between two Es lithotype levels. In these levels, intense silicification occurs in the shrubs and spherulites, and only sporadically in the matrix. In addition, there is a precipitation of late calcite replacing the clay minerals. The sample shows a milder and more localized intensity of these processes, with less replacement of the clay matrix. The argillaceous laminations are discontinued by the precipitation of carbonates (spherulites and shrubs). Locally, it is possible to individualize them into nodular aggregates and chaotic massive aggregates (Figure 4E). The SEM images show two compositions heterogeneously distributed in the matrix (Figure 4F).

The chemical compositions were determined by qualitative MEV-EDS analysis, and for this reason, the mineral formulas are approximations. The ideal compositions of kerolite, stevensite, and saponite are presented in Figure 5A, as well as Population 1, which is represented by sample 3085 (Figure 5B). The mineral formulas represent the obtained compositional range, and two compositions were identified as compatible with stevensite ($\text{Na}_{(0.16-0.31)}\text{Mg}_{(2.7-2.8)}\text{Si}_{(4.01-4.07)}\text{O}_{10}(\text{OH},\text{F})_2$) and kerolite ($\text{Mg}_{(2.8)}\text{Si}_{(4.08)}\text{O}_{10}(\text{OH},\text{F})_2$); these are reported in Table 1. Compositions compatible with stevensite were identified in sample 1515, with Na^+ in the interlayer position, and in sample 1955, with K^+ .

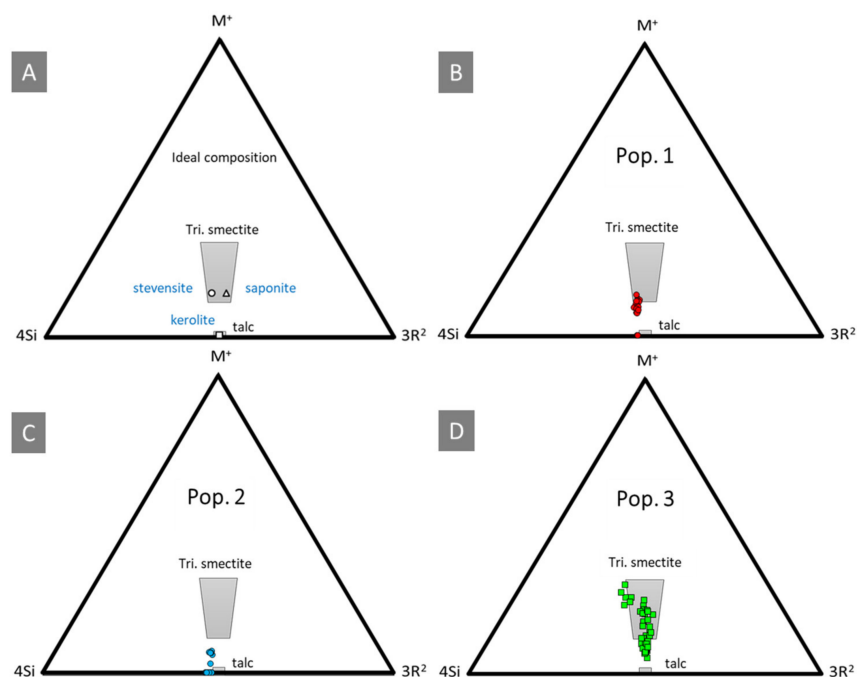


Figure 5. Trioctahedral clay compositions in the system $4\text{Si}-3\text{R}^{2+}-\text{M}^+$ [29]. (A) Ideal composition; (B) Population 1; (C) Population 2; and (D) Population 3. $4\text{Si} = \text{Si}^{4+}/4$; $\text{M} = \text{K}^+ + \text{Na}^+ + 2\text{Ca}^{2+}$; $3\text{R}^2 = \text{Mg}^{2+} + \text{Fe}^{2+}/3$.

Microanalyses of the clay minerals in samples 1515 and 1955 show a systematic excess of silica related to the silicification process that promoted the precipitation of microcrystalline silica in the interparticle porosity (Figure 4C).

The XRD diffraction patterns are very similar for the three samples, with a d_{001} value of 15.5 \AA for samples 1515 and 3085 for the reflection (001), and 14.7 \AA for sample 1955, which, after saturations with ethylene glycol, expanded to 16.9 \AA , characterizing them as smectites. In all three samples, there is a subordinate, broad reflection with leftward asymmetry at 9.5 \AA that could correspond to kerolite (Figure 6A).

In the heating tests at 490 and $550 \text{ }^\circ\text{C}$ of samples 1515 and 3085, the smectite collapsed, forming a wider reflection that joined that of the kerolite in the $9.9\text{--}10 \text{ \AA}$ region. In sample 1955, the smectite and kerolite structure collapsed, forming a diffuse band with low counts in the 9.6 \AA region. When saturated with ethylene glycol after heating, the behavior was different for each sample. Sample 1515 showed expansion after heating at $490 \text{ }^\circ\text{C}$. Sample 1955 showed no expansion, and sample 3085 showed a diffuse band in the 17 \AA region. Saturation in ethylene glycol of the samples heated to $550 \text{ }^\circ\text{C}$ did not cause expansion (Figure 6C).

The results showed that the smectites (stevensites) are irregularly interstratified with kerolite, with a wide predominance of the former. In modeling with Newmod[®], the results for these samples were: stevensite 85%, kerolite 15%, with $N = 7$ (Figure 6B).

In the 060 reflections of samples 1515 and 1955 (Figure 6A), a more intense band is noted in the region at $1.525\text{--}1.517 \text{ \AA}$ that may have been related to trioctahedral smectite, and in sample 3085, there is a peak at 1.525 \AA with asymmetry toward 1.52 \AA of trioctahedral character. In all three samples, a subordinate band occurs at $1.505\text{--}1.51 \text{ \AA}$ that could correspond to detritic dioctahedral minerals.

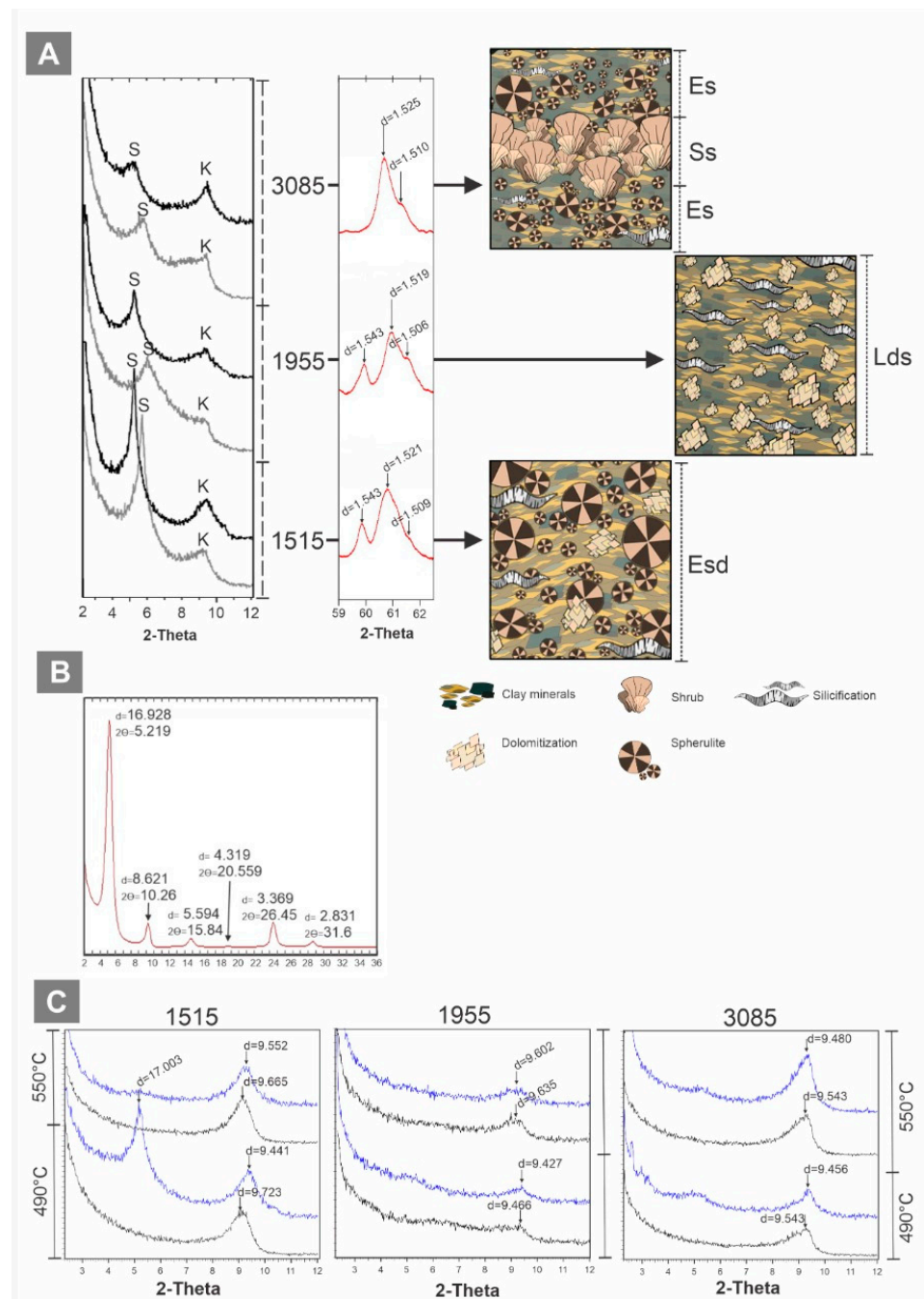


Figure 6. XRD patterns of clay minerals from different lithotypes (schematic representations) of Population 1: (A) <math><2\ \mu\text{m}</math>, 2–12 ®; (C) XRD patterns of heated samples to 490 and 550 °C (black) and EG-solvated after heating (blue) of the three samples. Es = spherulstone with silicification; Ss = shrubstone with silicification; Lds = laminate with dolomitization and silicification; Esd = spherulstone with silicification and dolomitization.

4.2.2. Population 2

Population 2 comprises three samples with a low degree of transformation of the pure syngenetic matrix, which is ubiquitous in the form of disseminated rhombohedral dolomite and locally microcrystalline silica. The clay minerals have a lamellar habit, yellowish-brown color, and high birefringence (3rd order), and are arranged in parallel aggregates forming the main lamination of the rock. The spherulites in these samples show local corrosive

microcrystalline dolomitization features at the edges of the constituents (Figure 7A) and microinclusions of clay minerals (Figure 7B).

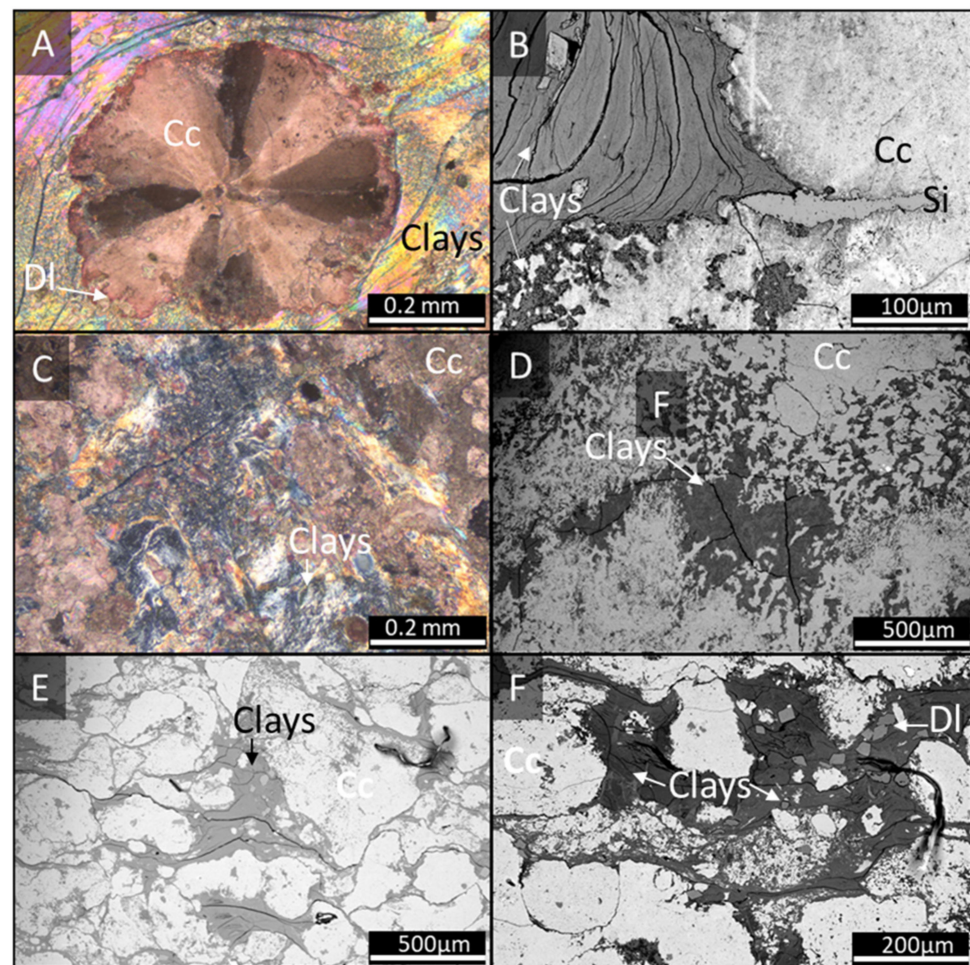


Figure 7. General aspects of Population 2. (A) Photomicrography of calcite spherulite recrystallized in triangular sectors with clay mineral inclusions and edges replaced by microcrystalline dolomite; (B) BSE image of the contact between clay matrix and spherulite with microinclusions of clay minerals and localized silicification; (C) photomicrography of heterogeneous transformation of the syngenetic laminated matrix by chaotic fibrous aggregates; (D) BSE image of heterogeneously distributed clay minerals; (E) BSE image of interstitial lamellar aggregates between spherulites; (F) BSE image showing two compositions of Mg clays (light gray and dark gray) partially replaced by dolomite and calcite. Cc = calcite; Si = silica; DI = dolomite.

Sample 3215 is composed of the intercalation of three lithotypes. Lithotype E occurs at the base, a peloidal level (P) with a lumpy texture in the intermediate portion, and lithotype S at the top. The intermediate level is intensely recrystallized by macrocrystalline calcite, and there is no preservation of clay material. In the E and S lithotypes, lamellar clay minerals of high birefringence (3rd order) are the most abundant. Locally, they are transformed to a chaotic low-birefringence aggregate (Figure 7C) that shows two compositions (light gray and dark gray) in the BSE images (Figure 7D).

Sample 3690 is composed only of lithotype E, and the highest amounts of clay minerals. In it, features of transformation from high-birefringence lamellar clay minerals to low-birefringence fibrous aggregates with chaotic orientation and slightly finer texture are observed in contact with spherulites.

Sample 3850 is composed only of lithotype E. However, these levels locally exhibit transitional forms between intensely amalgamated spherulites and spherulites. In these levels,

the predominant clay mineral is high-birefringence lamellar kerolite, the composition of which is shown in Table 1 and Figure 7E. Locally, two Mg clay compositions occur that are heterogeneously distributed (Figure 7F).

The clay compositions of Population 2 were determined by qualitative MEV-EDS, and are represented by sample 3850 (Figure 5C). They correspond mostly to kerolite, and punctually in some sites, minerals of stevensitic composition with interlayer Na^+ occur (Table 1). These minerals present a general formula compatible with kerolite ($\text{Mg}_{(2.7-2.8)}\text{Si}_{(4.08-4.15)}\text{O}_{10}(\text{OH},\text{F})_2$) and stevensite ($\text{Na}_{(0.06-0.15)}\text{Mg}_{(2.7-2.8)}\text{Si}_{(4.05-4.08)}\text{O}_{10}(\text{OH},\text{F})_2$).

The three samples show similar diffractograms, with reflections at 9.4–9.5 Å with leftward asymmetry in air-dried preparation and after saturation with ethylene glycol, corresponding to reflection (001) of kerolite (Figure 8A). In the heating tests at 490 and 550 °C, these minerals show no modifications, even when saturated with ethylene glycol after these tests.

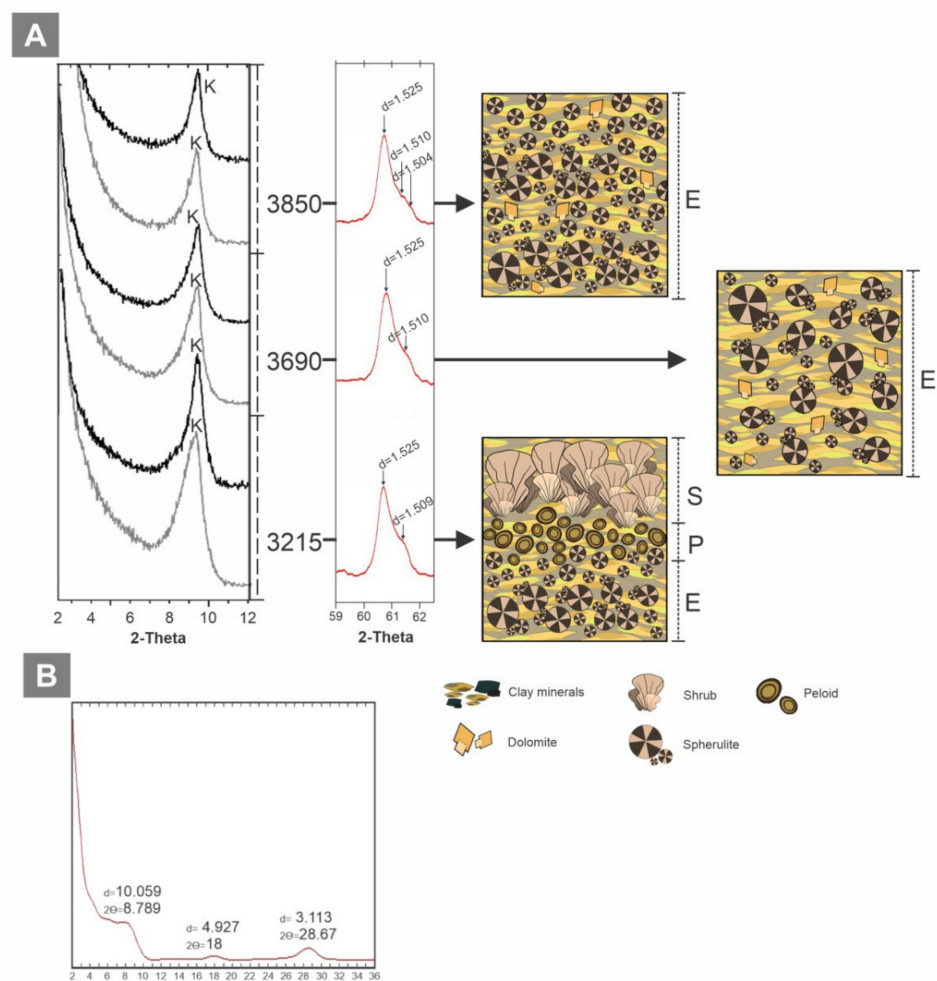


Figure 8. (A) XRD patterns of clay minerals from different lithotypes (schematic representations) of Population 2: $2-12\ 2\theta\ (d_{001})$ air-dried (gray) and EG-solvated (black), and $59-62\ 2\theta\ (d_{060})$; (B) XRD pattern obtained with Newmod®. E = spherulstone; S = shrubstone; P = peloidal level.

The reflection (060) of these samples shows a more intense, broad, asymmetric peak between 1.529–1.525 Å of kerolite, and a subordinate band in the region of 1.50–1.51 Å (Figure 8A).

The deconvolutions of the XRD patterns of the reflection (001) in the 9–10 Å region shows a more intense peak at 9.45 Å identified as pure kerolite, and another subordinate one at 10.0 Å. Population 2 was similarly modeled by Newmod®. The 10 Å reflection is of much lower intensity than the first at 9.45 Å. By applying Newmod®, an interstratification

with a wide predominance of kerolite (85%) with 15% stevensite for $N = 1$ was obtained for the second curve (Figure 8B).

4.2.3. Population 3

Population 3 comprises two samples that show a hybrid matrix with syngenetic clay minerals and detrital constituents such as quartz, micas, feldspars, and aluminous clay minerals (Figure 9A). In addition, the argillaceous levels are affected by partial replacement by microcrystalline calcite (Figure 9C,D).

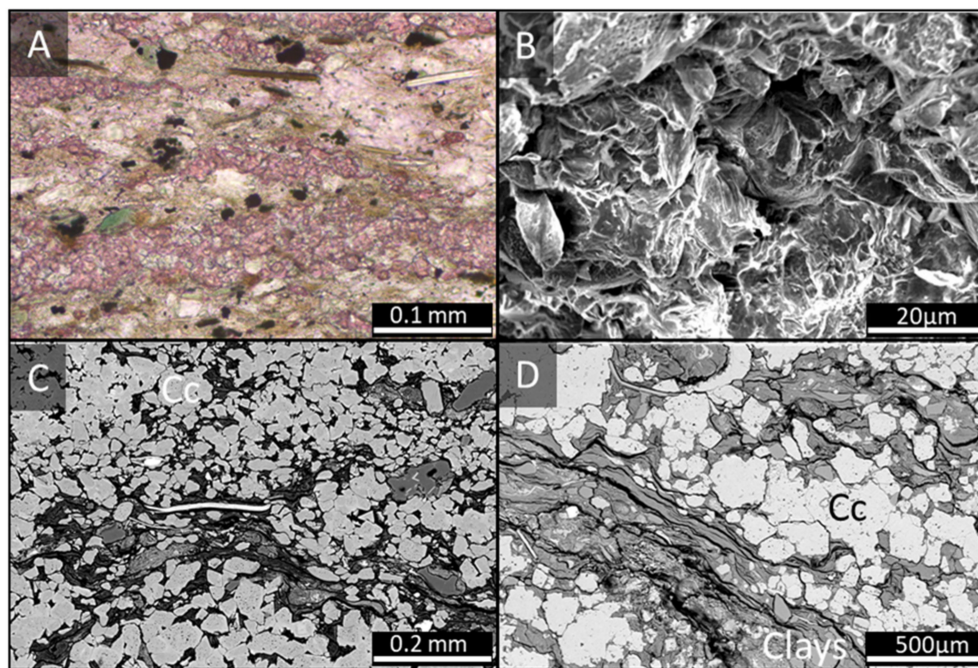


Figure 9. General aspects of Population 3: (A) photomicrography of the hybrid matrix composed of magnesian clay minerals, quartz, feldspar, mica, and massive green clay aggregates replaced by microcrystalline calcite (pink ink) and pyrite; (B) SE image of saponite aggregates; (C,D) BSE images showing levels of hybrid matrix heavily replaced by microcrystalline calcite.

Sample 3750 comprises L lithotype levels and an intermediate level composed exclusively of microcrystalline silica and microspherulitic chalcedony. The clayey levels are free of silicification and dolomitization processes. The syngenetic clay minerals show a lamellar habit, greenish-yellow coloration, and low (1st order) birefringence; form thin laminated aggregates (Figure 9B) parallel to the rock stratification; and consist of very fine particles mixed with the detrital constituents.

Sample 4415 is composed of a thin basal level of lithotype E cut by a millimeter-thick level of microcrystalline silica and microspherulitic chalcedony. Lithotype L also occurs, overlaying these levels. The syngenetic clay minerals have the same characteristics as sample 3750, but form slightly thinner levels with higher detrital mineral content, which result in significantly fewer clay minerals in this sample.

The clay compositions of Population 2 were determined by qualitative MEV-EDS and have a saponite composition (Table 1 and Figure 5D), with Al^{3+} and Fe^{2+} in the octahedron. The 3750 sample and the E lithotype of the 4415 sample have the same composition of $Na_{(0.05-0.5)}(Mg_{(2.4-3)}Fe_{(0.05-0.1)}Al_{(0-0.25)})(Si_{(3.6-3.9)}Al_{(0.1-0.4)})O_{10}(OH)_2$; and the L lithotype of 4415 have a different composition of $K_{(0.15-0.46)}Na_{(0.2-0.35)}(Mg_{(1.9-2.5)}Fe_{(0.15-0.36)}Al_{(0.15-0.44)})(Si_{(3.6-3.9)}Al_{(0.15-0.4)})O_{10}(OH)_2$.

The XRD analyses show very similar reflections between both samples, with reflection (001) at 15.1 Å in the air-dried oriented preparations and expansion to 16.9 Å after saturation with ethylene glycol, indicating the presence of smectite, and the discrete peak at 10.1 Å

indicating mica and/or illite (Figure 10A). In the heating tests at 490 and 550 °C, the smectite collapsed to 9.9 Å, preserving a band in the 12.4 Å region. When saturated with ethylene glycol after heating, its behavior was one of expansion for both temperatures, a behavior unique to this population (Figure 10B). In the reflection (060) of these samples, there is a main peak between 1.525 and 1.522 Å that could be related to trioctahedral smectite. However, this region presents other asymmetric and diffuse peaks, which could be attributed to the presence of reflections from calcite and other phases in smaller quantities, such as micas/illites.

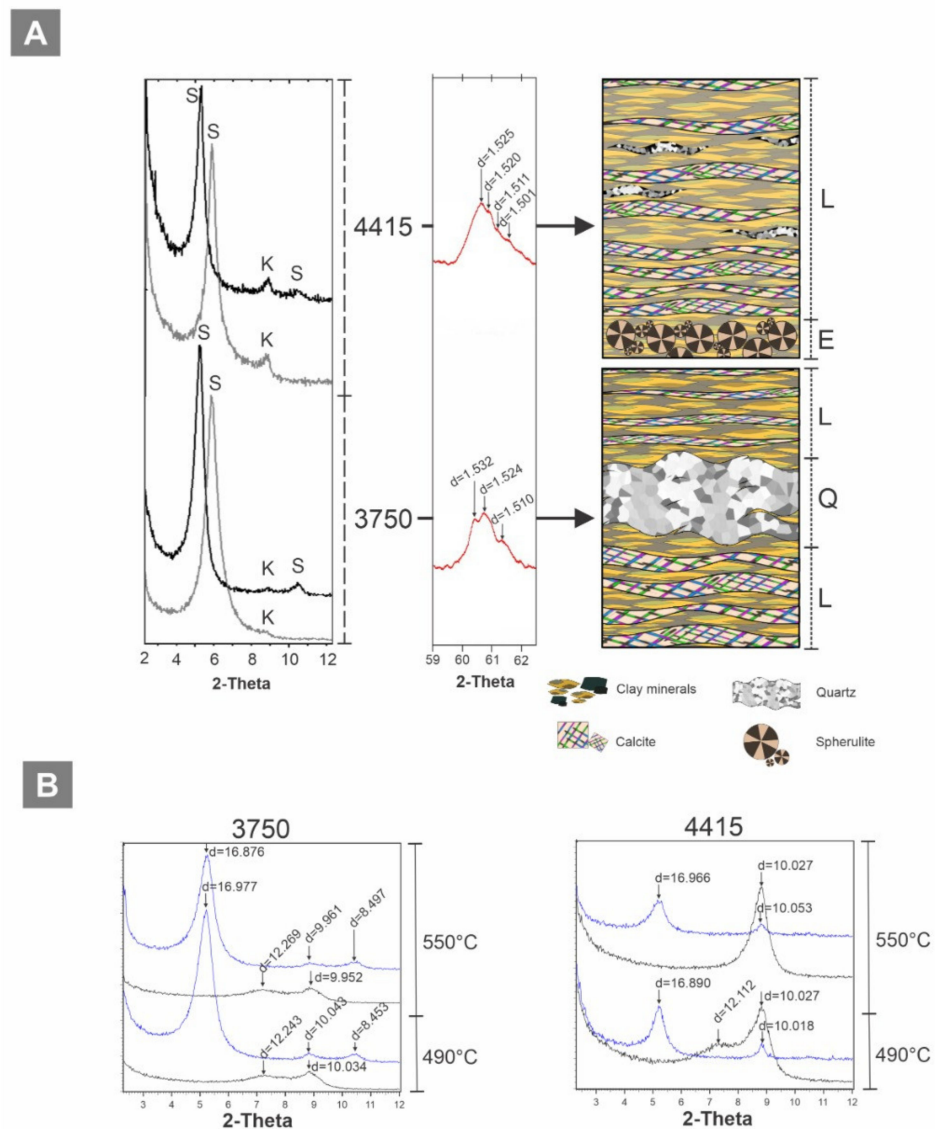


Figure 10. XRD patterns of clay minerals from different lithotypes (schematic representations) of Population 3: (A) $<2\ \mu\text{m}$ 2–12 2θ (d001) air-dried (gray) and EG-solvated (black), and 59–62 2θ (d060); (B) XRD patterns of heated samples to 490 and 550 °C (black) and EG-solvated after heating (blue). L = laminite; E = spherulite; Q = silica level.

5. Discussion

Magnesian clay minerals occur in a great diversity of environments, particularly in alkaline lacustrine. The different species reflect specific physicochemical conditions of the fluid, in addition to paleoenvironmental and paleoclimatic aspects.

Understanding the clay minerals in different contexts of these rocks requires answering two questions: (a) What are the clay minerals present in this interval? and (b) Which

processes and products can characterize the occurrence of the different species? These questions will be answered by integrating the results and interpreting the occurrences with the geochemical models proposed in the bibliography.

The predominant clay minerals in the borehole S2 are Al-free magnesian clays such as kerolite, Stv85/Ker15, and Ker85/Stv15, as well as locally saponites, following what has been described for the Barra Velha Formation [26]. The mixed layers were identified by XRD, and through modeling of their diffraction pattern, were defined as Ker85/Stv15 ($N = 1$) and Stv85/Ker15 ($N = 7$), which have a low interlayer charge and systematically plotted in the intermediate field between the composition of talc and trioctahedral smectites [29].

These Mg-clay minerals are considered to form in suspension by syngenetic precipitation in the water column and deposit in a low-energy environment eventually composed of fine terrigenous constituents from the lacustrine margin. This understanding is supported by the preservation of primary rock lamination, which is subsequently displaced and disrupted by the precipitation of microcrystalline calcite, spherulites, and shrobs in these sediments in early diagenesis, before compaction. However, this precipitation did not significantly transform the lamellar clay aggregates, even when they were included within the carbonates. Therefore, the lithotypes do not represent the variations of clay minerals species.

Diagenetic constituents such as dolomite and silica are post-products of calcite precipitation, and locally replace carbonates and clay minerals. The spherulites locally show corrosion and substitution features of their rims by dolomite and silica. These processes, when more intense, cause the transformation of the residual clay minerals. This is the case of the mineral assemblages present in Population 1, in which banded microcrystalline silica and microcrystalline dolomite intensely replace the lamellar aggregates composed of kerolite. These processes in this population result in the presence of heterogeneously distributed non-lamellar aggregates of a Stv85/Ker15 mixed layer that occur in greater proportion in the samples with a higher degree of transformation. The dissolution of clay minerals changes the interparticle fluid composition, and can result in the dolomite precipitation and the silicification observed in these rocks [8].

In Population 2, lamellar aggregates of kerolite predominate. The matrix substitution processes are punctual, not very intense, and form rhombohedral dolomite and/or macrocrystalline quartz. Locally, the lamellar aggregates are transformed into non-laminate Ker85/Stv15 aggregates that are heterogeneously distributed in the matrix.

The laminated matrix of Population 3 is replaced and discontinued by microcrystalline calcite laminations; chaotic aggregates, dolomite, and quartz do not occur. The clay levels are composed of detrital constituents, and the syngenetic matrix is made of saponite.

The presence of kerolite in Populations 1 and 2 indicates authigenesis by direct precipitation from solutions or gel from lake water under conditions of high Mg/Si ratios, pH below 9, and high salinity [30]. The transformation of kerolite results in the formation of Ker85/Stv15 mixed layers, which should occur by increasing pH at diagenesis. A similar process gives rise to the Stv85/Ker15 mixed layer in Population 1, but in a more intense matrix-transformation condition, as observed in samples 1515 and 1955. The saponites of Population 3 possibly represents a mixture of lake and stream water. Their formation is controlled by the composition of the detrital sediments rich in Al^{3+} , K^+ , and Fe^{2+} , creating conditions for transformation or authigenic precipitation [30]. This population indicates episodes of increased input of inherited sediments to the lake, and in these contexts, the clay transformation mechanism is favored [31].

The large-scale occurrence of these magnesian silicates and carbonates may be associated with volcanic environments, and the tholeiitic basalts of Paraná-Etendeka Province could be this source [32]. The hypothesis of mantle serpentinization has also been raised as a possible source of the Mg^{2+} , Si^{4+} , and Ca^{2+} present in the formation environment of these rocks [26,33].

Farias et al. [12] proposed an evaporative model for the Santos Basin with the influence of hydrothermal fluids related to Walvis Ridge. Evaporation can be the mechanism able to control the high salinity of lake water and trigger the precipitation and deposition of low-crystallinity Mg silicates. It results in calcite precipitation in the lake substrate as a function of the high saturation in calcium carbonate generated by the consumption of Mg^{2+} and Si^{4+} under the appropriate PCO_2 conditions [7,19]. The alternation of spherulite and shrub precipitation may represent geochemical fluctuations of the lake caused by evaporation and variations in the fluid Mg^{2+} and Si^{4+} consumption [26].

6. Conclusions

The precipitation of different carbonate morphologies and lithotypes does not exert significant influence in the variations in the associated magnesian clay species. The key control on the precipitated magnesian silicates is the composition of the water from which these minerals formed, as is the case of saponite that occurs in episodes of greater sedimentary input to the lake, and kerolite and Ker/Stv mixed layers in periods without this influence.

Kerolite is the most abundant clay mineral in the sampled interval, and occurs as lamellar aggregates of high birefringence that constitute the lamination of the rock, free of transformation processes.

The Ker85/Stv15 mixed layer occurs as a localized product of kerolite transformation associated with rhombohedral dolomite and macrocrystalline quartz.

The Stv85/Ker15 mixed layer occurs as non-laminated aggregates heterogeneously distributed in the carbonate interstices from kerolite transformation. These aggregates predominate where the dolomitization and silicification processes are more intense and widespread.

Author Contributions: Conceptualization, M.D.d.S. and M.E.B.G.; Data curation, M.D.d.S., M.E.B.G., S.M.D., L.A.C.S., L.B.G. and C.C.P.; Formal analysis, M.D.d.S. and M.E.B.G.; Investigation, M.D.d.S., M.E.B.G., A.S.M., M.P., L.A.C.S., P.N. and D.D.; Methodology, M.D.d.S., M.E.B.G., A.S.M. and L.A.C.S.; Resources, M.D.d.S.; Software, M.D.d.S., A.S.M. and N.D.; Supervision, M.E.B.G., A.S.M., M.P., P.N., J.F.S. and C.W.D.R.; Writing—original draft, M.D.d.S.; Writing—review & editing, M.D.d.S., M.E.B.G., A.S.M., S.M.D. and R.S.C. All authors have read and agreed to the published version of the manuscript.

Funding: This research was funded by PETROBRAS through a cooperation agreement (SAP: 4600569731—Legal Number: 5850.0107216.18.9—Process 2017/00168-0) associated with the project: “Study and Characterization of Pre-Salt Clay Levels and Analogues”.

Acknowledgments: We are grateful to PETROBRAS, for permission to publish this paper and for supporting this study, and to CPGQ-IGEO-UFRGS for all their support and the use of their laboratories. We also thank the two anonymous reviewers who allowed this paper to be greatly improved.

Conflicts of Interest: The authors declare no conflict of interest.

References

1. Pozo, M.; Galán, E. Magnesian clay deposits: Mineralogy and origin. In *Magnesian Clays: Characterization, Origin and Applications*; Pozo, M., Galán, E., Eds.; Digilabs: Bari, Italy, 2015; pp. 175–227.
2. Khoury, H.N.; Eberl, D.D.; Jones, B.F. Origin of Magnesium Clays from the Amargosa Desert, Nevada. *Clays Clay Miner.* **1982**, *30*, 327–336. [[CrossRef](#)]
3. Benhammou, A.; Tanouti, B.; Nibou, L.; Yaacoubi, A.; Bonnet, J.P. Mineralogical and physicochemical investigation of mg-smectite from jbel ghassoul, Morocco. *Clays Clay Miner.* **2009**, *57*, 264–270. [[CrossRef](#)]
4. Pozo, M.; Calvo, J.P. Madrid Basin (Spain): A natural lab for the formation and evolution of magnesian clay minerals. In *Magnesian Clays: Characterization, Origin and Applications*; Pozo, M., Galán, E., Eds.; Digilabs: Bari, Italy, 2015.
5. Jones, B.F.; Galan, E. Sepiolite and Palygorskite. *Rev. Mineral. Geochem.* **1988**, *19*, 631–674.
6. Ceraldi, T.S.; Green, D. Evolution of the South Atlantic Lacustrine deposits in response to Early Cretaceous rifting, subsidence and lake hydrology. In *Petroleum Geoscience of the West African Margin*; Ceraldi, T.S., Hodgkinson, R.A., Backe, G., Eds.; Geological Society: London, UK, 2016.

7. Herlinger, R.; Zambonato, E.E.; De Ros, L.F. Influence of diagenesis on the quality of lower cretaceous pre-salt lacustrine carbonate reservoirs from northern Campos Basin, Offshore Brazil. *J. Sediment. Res.* **2017**, *87*, 1285–1313. [[CrossRef](#)]
8. Lima, B.E.M.; De Ros, L.F. Deposition, diagenetic and hydrothermal processes in the Aptian Pre-Salt lacustrine carbonate reservoirs of the northern Campos Basin, offshore Brazil. *Sediment. Geol.* **2019**, *383*, 55–81. [[CrossRef](#)]
9. Leite, C.O.N.; Silva, C.M.A.; De Ros, L.F. Depositional and diagenetic processes in the pre-salt rift section of a Santos Basin Area, SE Brazil. *J. Sediment. Res.* **2020**, *90*, 584–608. [[CrossRef](#)]
10. Souza, R.S.; Arienti, L.M.; Viana, S.M.; Falcao, L.C.; Cuglieri, M.A.; Silva, R.P.; Leite, C.O.; Oliveira, V.C.; Oliveira, D.M.; Anjos, C.; et al. Petrology of the hydrothermal and evaporitic continental Cretaceous (Aptian) pre-salt carbonates and associated rocks, South Atlantic Santos basin, offshore Brazil. In Proceedings of the AAPG/ACE Annual Convention & Exhibition, Salt Lake City, UT, USA, 19–22 May 2018.
11. Madrucci, V.; Araújo, C.C.; Anjos, C.W.D.; Spadini, A.R. Depositional paleoenvironment of authigenic magnesium clays in pre-salt of Santos Basin—Brazil. In Proceedings of the 16th International Meeting of Carbonate Sedimentologists, Bathurst Meeting Mallorca, Palma de Mallorca, Spain, 9–11 July 2019; p. 152.
12. Farias, F.; Szatmari, P.; Bahniuk, A.; França, A.B. Evaporitic carbonates in the pre-salt of Santos Basin—Genesis and tectonic implications. *Mar. Pet. Geol.* **2019**, *105*, 251–272. [[CrossRef](#)]
13. Almeida, F.F.M.; Neves, B.B.B.; Carneiro, C.D.R. The origin and evolution of the South American Platform. *Earth-Sci. Rev.* **2000**, *50*, 77–111. [[CrossRef](#)]
14. Milani, E.J.; Rangel, H.D.; Bueno, G.V.; Stica, J.M.; Winter, W.R.; Caixeta, J.M.; Neto, O.C.P. Bacias Sedimentares Brasileiras, Cartas Estratigráficas. *Bol. De Geociências Da Petrobras* **2007**, *15*, 183–205.
15. Moreira, J.L.P.; Madeira, C.V.; Gil, J.A.; Machado MA, P. Bacia de Santos. *Bol. Geosci. Petrobras* **2007**, *15*, 53–549.
16. Dias, J.L.; Oliveira, J.Q.; Vieira, J.C. Sedimentological and stratigraphic analysis of the Lagoa Feia Formation, rift phase of Campos basin, offshore Brazil. *Rev. Bras. De Geociências* **1988**, *18*, 252–260. [[CrossRef](#)]
17. Dias, J.L. Análise Sedimentológica e Estratigráfica do Andar Aptiano em Parte da Margem Leste do Brasil e no Plato das Malvinas, Considerações Sobre as Primeiras Incursões e Ingressões Marinhas do Oceano Atlântico Sul Meridional. Ph.D. Thesis, Universidade Federal do Rio Grande do Sul, Porto Alegre, Brazil, 1998.
18. Terra, G.J.S.; Spadini, A.R.; Franca, A.B.; Sombra, C.L.; Zambonato, E.E.; Juschaks, L.C.S.; Arienti, L.M.; Erthal, M.M.; Blauth, M.; Franco, M.P.; et al. Classificação de rochas carbonáticas aplicável às bacias sedimentares brasileiras. *Bol. Geocienc. PETROBRAS* **2010**, *18*, 9–29.
19. Wright, V.P.; Barnett, A.J. An abiotic model for the development of textures in some South Atlantic early Cretaceous lacustrine carbonates. *Geol. Soc. Spec. Publ.* **2015**, *418*, 209–219. [[CrossRef](#)]
20. Sartorato, A.C.L. Caracterização faciológica, estratigráfica e diagenética dos reservatórios carbonáticos da Formação Barra Velha, Bacia de Santos. Master's Thesis, UERJ, Rio de Janeiro, Brazil, 2018.
21. Wright, V.P.; Barnett, A.J. The textural evolution and ghost matrices of the Cretaceous Barra Velha Formation carbonates from the Santos Basin, offshore Brazil. *Facies* **2020**, *66*, 1–18. [[CrossRef](#)]
22. Gomes, J.P.; Bunevich, R.B.; Tedeschi, L.R.; Tucker, M.E.; Whitaker, F.F. Facies classification and patterns of lacustrine carbonate deposition of the Barra Velha Formation, Santos Basin, Brazilian Pre-salt. *Mar. Pet. Geol.* **2020**, *113*, 104176. [[CrossRef](#)]
23. Goldberg, K.; Kuchle, J.; Scherer, C.; Alvarenga, R.; Ene, P.L.; Armententi, G.; De Ros, L.F. Re-sedimented deposits in the rift section of the Campos Basin. *Mar. Pet. Geol.* **2017**, *80*, 412–431. [[CrossRef](#)]
24. Rehim, H.A.A.A.; Mizusaki, A.M.P.; Carvalho, M.D.; Monteiro, M. Talco e Estevensita na Formação Lagoa Feia da Bacia de Campos—Possíveis implicações no ambiente deposicional. In Proceedings of the Anais XXXIV Congresso Brasileiro de Geologia, Goiânia, Brazil, 12 October 1986; pp. 416–424.
25. Bertani, R.T.; Carozzi, A.V. Lagoa Feia Formation (Lower Cretaceous), Campos Basin, offshore Brazil: Rift valley stage lacustrine carbonate reservoirs, I. *J. Pet. Geol.* **1985**, *8*, 37–58. [[CrossRef](#)]
26. Tosca, N.J.; Wright, V.P. Diagenetic pathways linked to labile Mg-clays in lacustrine carbonate reservoirs: A model for the origin of secondary porosity in the Cretaceous pre-salt Barra Velha Formation, offshore Brazil. In *Reservoir Quality of Clastic and Carbonate Rocks: Analysis, Modelling and Prediction*; Armitage, P.J., Butcher, A.R., Churchill, J.M., Csoma, A.E., Hollis, C., Lander, R.H., Omma, J.E., Worden, R.H., Eds.; Geological Society: London, UK, 2015; Volume 435, pp. 33–46.
27. Christidis, G.E.; Koutsopoulou, E. A simple approach to the identification of trioctahedral smectites by X-ray diffraction. *Clay Miner.* **2013**, *48*, 687–696. [[CrossRef](#)]
28. Reynolds, R.C., Jr. *NEWMOD(R)®: A Computer Program for the Calculation of One-Dimensional Diffraction Patterns of Mixed-Layer Clays*; Reynolds, R.C., Jr., Ed.; 8 Brook Dr.: Hanover, NH, USA, 1985.
29. Meunier, A.; Inoue, A.; Beaufort, D. Smectite-to-chlorite conversion series from the Ohyu caldera, Japna. *Clays Clay Miner.* **1991**, *39*, 409–415. [[CrossRef](#)]
30. Pozo, M.; Calvo, J.P. An overview of authigenic magnesian clays. *Minerals* **2018**, *8*, 520. [[CrossRef](#)]
31. Calvo, J.P.; Blanc-Valleron, M.M.; Rodríguez-Aranda, J.P.; Rouchy, J.M.; Sanz, M.E. Authigenic clay minerals in continental evaporitic environments. In *Palaeoweathering, Palaeosurfaces and Related Continental Deposits*; Thiry, M., Simon-Coignon, R., Eds.; Special Publications of the International Association of Sedimentologists: Oxford, UK, 1999; pp. 129–151.

-
32. Wright, V.P. Lacustrine carbonates in rift settings: The interaction of volcanic and microbial processes on carbonate deposition. In *Advances in Carbonate Exploration and Reservoir Analysis*; Garland, J., Neilson, J.E., Laubach, S.E., Whidden, K.J., Eds.; Geological Society: London, UK, 2012; Volume 370, pp. 39–47.
 33. Pinto, V.H.G.; Manatschala, G.; Karpoffa, A.M.; Ulricha, M.; Viana, A.R. Seawater storage and element transfer associated with mantle serpentinization in magma-poor rifted margins: A quantitative approach. *Earth Planet Sci.* **2017**, *459*, 227–237. [[CrossRef](#)]